Tribological Challenges of Scaling Up Tidal Turbine Blades

Shayan Sharifi, Cameron Johnstone and Margaret M. Stack

Department of Mechanical & Aerospace Engineering, University of Strathclyde
Glasgow, UK
Shayan.Sharifi@strath.ac.uk
Cameron.Johnstone@strath.ac.uk
Margaret.Stack@strath.ac.uk

***Abstract*– Generating electricity from renewable resources (wind, wave and tidal) is of increasing interest. Of all marine renewables, tidal energy, by comparison, possesses the higher persistency and predictability over long time scales and the higher density of water than air results in greater power output from a tidal turbine than a wind turbine with similar dimensions. However, due to the nature of the tides, developing a reliable device for such environments, especially with an increased rotor diameter, raises more challenges to be addressed including the tribological challenges such as sediment erosion, cavitation erosion and their possible synergistic effects on the tidal turbine blades. This research focuses on testing and developing materials for improved tribological performance in tidal environments. This includes producing a variety of composite materials with different fibres and layouts reinforcement to evaluate two main tribological issues of composite materials in tidal environments: matrix cutting and reinforcement fracture using a loped test rig, which measures the effects of impact angle, particle size and concentrations at different tip speeds. The test samples are analysed using scanning electron microscopy (SEM) to conduct a surface topography and characterisation.**

***Keywords*——**Tidal turbine blades, composite materials, Erosion, particle erosion, impact angles.

I. INTRODUCTION

Offshore renewable energy resources in the world can potentially provide up to 330,000 terawatt hours electricity per year [1]. This has brought extensive attention in marine technologies including wind, wave and tidal. Despite major investment and development in offshore wind technology devices, for the wave and tidal sector, and many designs under development, there is still no agreement on the optimum material design for best performance. This is possibly due to the general lack of understanding of the performance of materials in such environments. The cost of the generated energy is one of the main drivers of selection of a harnessing technology and offshore wind is currently the most advanced of the marine renewable technologies. The various relative advantages of tidal energy however, such as persistency and predictability, over the other renewables over long time scales due to the well documented behaviour of the tides, currently make tidal technology favourable, if material performance can be optimized. Also, due to the higher density of water than air, a greater power output is expected from a tidal turbine comparing with a wind turbine with similar dimensions in comparable fluid flow velocities [2].

One of the main current barriers of tidal energy technologies is the reliability of the materials used for such devices which can increase the operational and maintenance costs. Hence, using more reliable but cheaper materials can be a method of reducing the cost of generating energy for this technology. Horizontal axis tidal turbines are a type of tidal energy devices that convert the kinetic energy of the flowing water into rotational motion and generate electricity using a generator. Although the blades of this type of turbines use aerodynamic profiles, the shape of the blades are different from wind turbine blades and designed to rotate in both directions. Taking this into consideration, as well as the higher density of water and the aggressive environment of the sea, requires a material with remarkable longevity under such conditions.

The desirable mechanical properties, corrosion resistance and generally cost effectiveness of fibre reinforced composite materials make them an attractive choice for this purpose. However, due to the nature of the tides, identifying a reliable composite material for such environments, especially with an increased rotor diameter, raises more issues to be addressed including the tribological challenges such as sediment erosion, cavitation erosion and their possible synergistic effects on the tidal turbine blades [3]. This research focuses on testing and identifying materials with a better tribological performance in tidal environments. This includes producing a variety of composite materials with different fibres and layouts reinforcement to evaluate two main tribological issues of

composite materials in tidal environments: matrix cutting and reinforcement fracture [4] using a loped test rig. At this stage of the research, commercially available materials have been tested in order for the authors to be able to validate the test results with the data available in the literature as the testing method is purposefully modified to (partially) replicate the tidal environment conditions. GFRP composites are generally the most popular materials used for cost effective turbines. This is also due to the good structural properties of this type of composites. The testing material for this work is the National Electrical Manufacture Association (NEMA) G10 epoxy glass laminate which is widely used in electrical equipment, aerospace conditions, medical diagnostic and underwater conditions. This thermosetting industrial composite consists of continuous filament glass cloth and epoxy as the resin binder. The general characteristic of this material is the high strength, low moisture absorption and excellent chemical resistance in dry and humid conditions. G10 is well suited to applications where high surface hardness is required.

In this study G10 epoxy glass laminate samples will be tested for its erosion resistance under the sub-sea conditions. The results of this work will be used to compare with tribological performance of different types of composite materials in the future stages of this research project.

II. EXPERIMENT DETAILS

A. Test Samples

The test samples in these experiments functioned as blades of a propeller. Thus, the samples were cut into a suitable size for the test rig in a rectangular shape. The final dimensions of the tests samples were 60 mm and 25 mm in length and breadth with the thickness of 6 mm. The sample specifications are listed in Table 1. The sides of the rectangular specimens were polished using 1200 grit SiC papers to ensure a high quality surface finish and eliminate the susceptibility of the occurrence of erosion from the sides as they were not the sites of interest of the tests.

G10 sample properties	
Flexural strength (MPa)	482
Tensile strength (MPa)	320
Shear strength (MPa)	131
Impact (Notched CHARPY) (kJ/m^2)	65
Density (kg/m^3)	2000
Specific gravity	1.82
Water absorption (mg)	0.8
Hardness, Rockwell (m-scale)	110
Standard finish	Satin/Glossy
Body colour	Green

Table 1 – Properties of the G10 specimens

Then the samples were cleaned by methanol wipes to remove the dust. This was carried out carefully to avoid creating scratches on the surfaces. After ensuring the dryness of the samples, the initial weights of the samples were measured 3 times to avoid reading errors.

B. Test Slurry

The tests were conducted using three different types of slurry to investigate the influences of different components. The test solutions used were salt water with the a salinity similar to the sea water (3.5 wt%), silica sand only in the water with the concentration of 3 wt% and the salt + silica sand solution using the same concentrations. The sand particles were sieved twice in the lab to ensure that the size distribution of the particles is accurate. The chemical composition of the sand used to produce the solutions is reported in Table 2. The specific gravity and uncompacted bulk density of the particles were 2.65 and 1.56 respectively. It should be noted that the concentration of the silica sand defines the density of the slurry where higher concentration provides higher density and requires more energy for the suspension. Higher concentrations also cause the distribution of the particles to become uneven [5]. Therefore, a concentration similar to the seabed environment was chosen and kept constant. The size distribution of the sand particles was chosen to be medium according to the U.S. Geological Survey Open-File Report 2006-1195 which is ranged from 250-500 µm.

Chemical composition of the silica sand (%)						
SiO_2	Fe_2O_3	Al_2O_3	K_2O	CaO	Na_2O	LOI
99.72	0.048	0.07	0.02	<0.01	0.04	0.05

Table 2 – Chemical composition of the sand particles

C. Test Apparatus

The test rig used for this set of experiments was a modified slurry pot tester. The rig consisted of a test chamber and two motors at the top and the bottom of the rig that provide the rotational motion of two propellers which functioned as a miniature turbine and a stirrer respectively. Figure 1 is an image of the test rig in a stationary mode and Figure 2 illustrates the test chamber showing the inserted test samples and the direction of the flow motion. The slurry pot tester investigates the erosion resistance of different materials rapidly and inexpensively.

The test samples which functioned as the turbine blades were inserted in different angled slots on a sample holder which acted as the hub of the turbine. A number of hubs were manufactured to test the samples in different impact angles. The slots on the hubs were spaced by 15^o from 0 – 90^o. The

role of the baffles in the test chamber were to prevent unwanted swirling of the flow due to the rotation of the samples and while the bottom propeller stirred the solution and provided the longitudinal flow and a good mixing of the slurry [6]. The propellers were rotating in opposite directions to avoid random motion of the particles, turbulence of the flow and error in the calculation of the impact velocity [5]. The blades of the bottom four bladed propeller (stirrer) were pitched at 45^{o} which is the optimal degree to provide a better particle distribution. Also, down-pumping (which was used in the tests) has been found to supply a more uniformed suspension and distribution of the particles [7]. The rotational velocities of the propellers were controlled using the controllers shown in Figure 1.

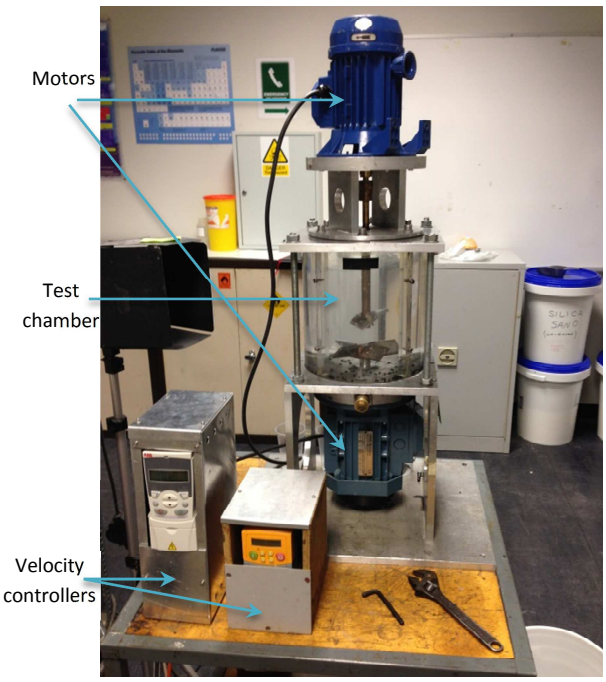

Figure 1 – Test apparatus

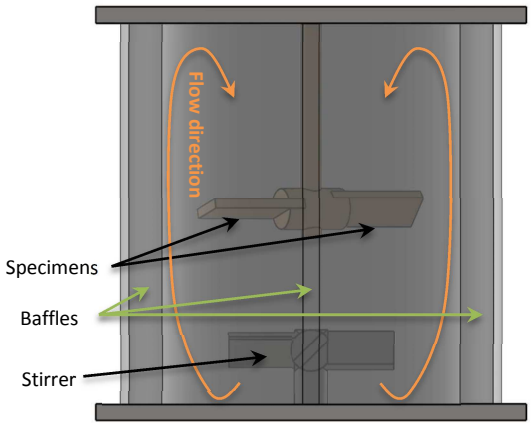

Figure 2 – Test chamber

D. Test Methodology

The tests were conducted to measure the effects of impact angles in different solutions. In order to measure the effects of the impact angles, the samples were tested at seven different angles. It is reported that orientation angle of the test specimens can be considered as the impact angle of the sand particles [7]. Also, Tsai et al. have reported that the presence of vortices can affect the test results from a slurry pot tester and they recommended employing lower velocities for the rotation of the specimen [8]. This was empirically tested by the current authors. The flow motion of the slurry was investigated using a high speed camera and large polymer particles and the suitable velocities were chosen for the experiments. For this set of tests, the tip speed of 3 m/s was chosen and the flow was completely following the directions that are shown in Figure 2. The tip speed was constantly probed and the motor power was adjusted accordingly to provide a constant velocity for all the impact angles tested. Using the high speed camera the trajectory of the particles was confirmed to be following the flow motion direction.

In this type of test configuration, uniform distribution of the sand particles is very important and controlled by the speed of the stirrer. Although it may be thought that the higher speed of the stirrer can provide a better suspension, this can cause a turbulent flow and appearance of vortices [5]. Therefore, once the full suspension of the particles was observed, the speed of the stirrer was recorded and kept constant for the whole set of the experiments. The constant speed of the stirrer was 309 rpm which was equal to 11 Hz of the bottom motor output. Three different solutions were used for the tests: salt water, sand only in the water and sand + salt in the water. The tests were conducted in the room temperature. The test chamber was completely filled with the solutions to eliminate the appearance of bubbles from the residual air in the chamber and avoid their disturbance. The solutions that contained silica sand were replaced every half an hour to minimise the attrition of the sand particles. The attrition of the sand particles after half an hour was found to be 2.59 wt% on average.

Test parameters	
Impact angles	0, 15, 30, 45, 60, 75 and 90^{o}
Solutions	Salt only, Sand only and Sand + Salt
Salinity (wt%)	3.5
Sand concentration (wt%)	3
Test duration (hrs)	2
Sand particles size (µm)	250 – 500
Linear tip speed (m/s)	3

Table 3 – Test parameters

The duration of each test was 2 hours and this was chosen in accordance with the tests reported in the literature in order to keep the comparability of the results. After completing each test, the samples were taken out, dried and cleaned using methanol wipes and kept under a gentle heat for 15 minutes. The weight measurements were carried out the day after the tests to minimise the errors from the wettability of the samples. Table 3 lists the tests specifications.

III. RESULTS

A. Weight variations

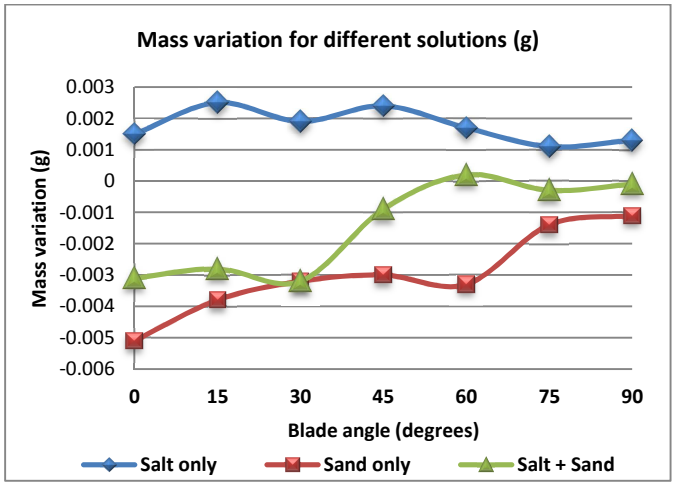

Figure 3 – Weight variation of the specimens

The weight of the specimens were measured with the accuracy of 10^{-4}g and it was found that the specimens from the tests with salt only solutions have gained weight whereas a weight loss was observed for almost all of the tests performed in the other solutions. The weight variations of the samples at different impact angles are plotted in Figure 3.

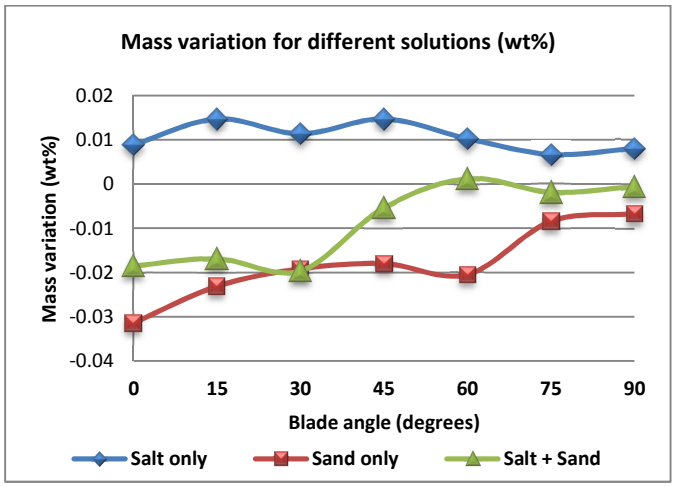

Figure 4 – Wt% variation

Although the initial weight of the samples were very close to each other, in order to normalise the results and compare the effects of the different impact angles on the mass variation, the results are plotted in wt% in Figure 4. The results indicate that lower impact angle have shown more interaction with the solutions and the solid particles. Higher weight gain and weight loss have taken place in the lower impact angles and this is similar for all of the solutions. It should be noted that although the results show a higher mass loss for the sand only solution, the weight gain due to the presence of the salt in the sand + salt solution should be taken into consideration. This is discussed in detail in the next section.

B. SEM micrographs

Following the weight measurement, the specimens were taken to scanning electron microscopy (SEM) to inspect the surface of specimens. The images were taken using a S3700 (Hitachi, Japan) Tungsten Filament Scanning Electron Microscope. As the samples were non-conductive, the inspection surfaces were gold coated prior to the analysis to increase the clarity of the images. Figure 5 is a close view of a fresh sample before the test. The faded brighter areas can be trapped micro-bubbles under the glossy surface or the residual dust from the side surface finishing as the surfaces were wiped very gently afterwards. It should be noted that as the samples were purchased from a commercial supplier, some tiny dents and superficial scratches were observed which can be due to the transportation. Extra care was taken to use the samples for the tests with a surface finish close to perfect.

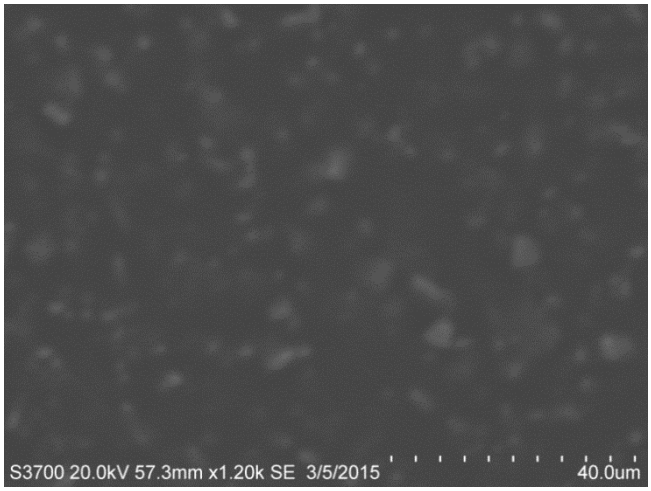

Figure 5 – A close view of a fresh surface

Figure 6 exhibits three different sites of the specimen used in the salt solution with the 60^{o} of impact angle. Figure 6(a) shows a wider view of the surface after the tests and shows the salt crystals dried on the surface. In a closer view it can be

seen that any defects on the surface can increase the amount of the accumulated salt on the surface (Figure 6(b)). As the glass cloth fibres were woven in 0 and 90^{o} directions, the last layer of the glass fibres in one direction was closer to the surface and caused some imperfection on the surface.

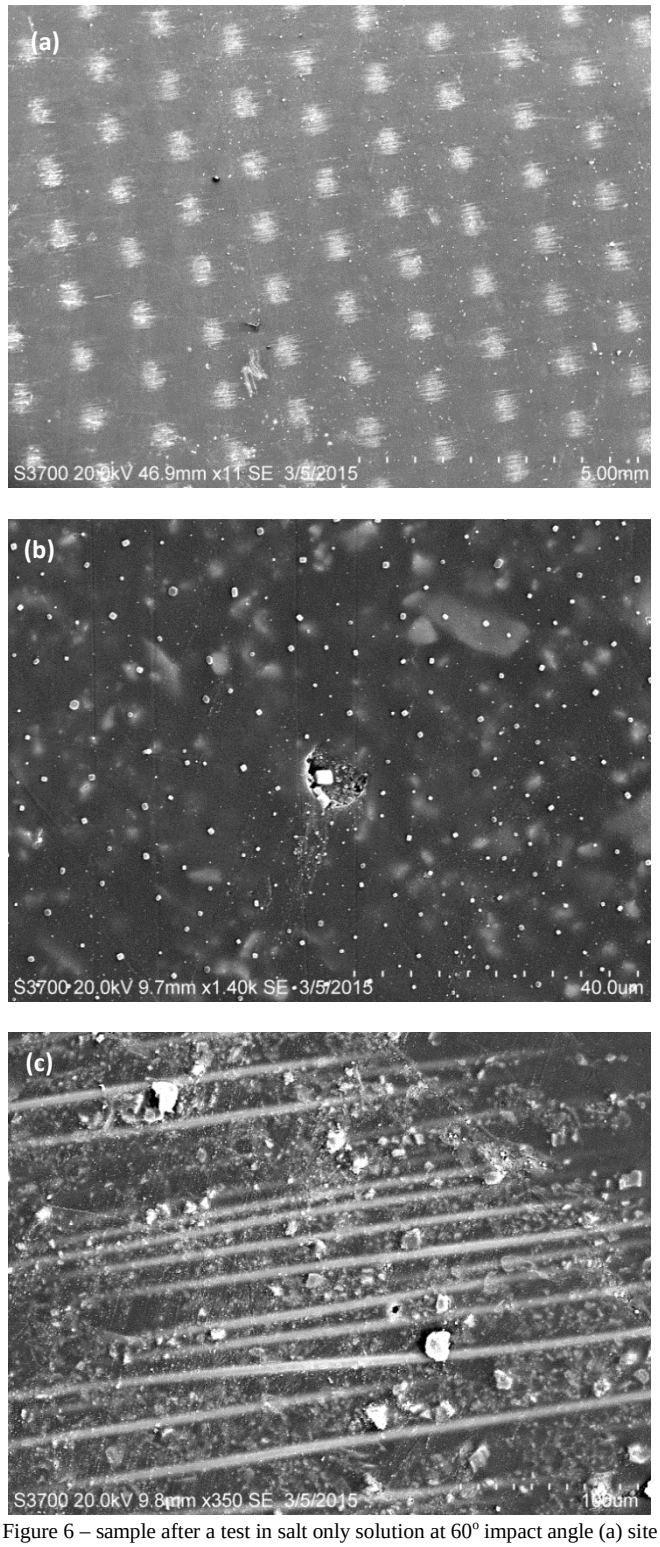

Figure 6 – sample after a test in salt only solution at 60^{o} impact angle (a) site 1, (b) site 2 and (c) site 3

As it can be observed in Figure 6(c), these areas absorb more salt crystals as they can be accumulated better in those areas. This phenomenon was observed on the other samples tested in the salt only solution.

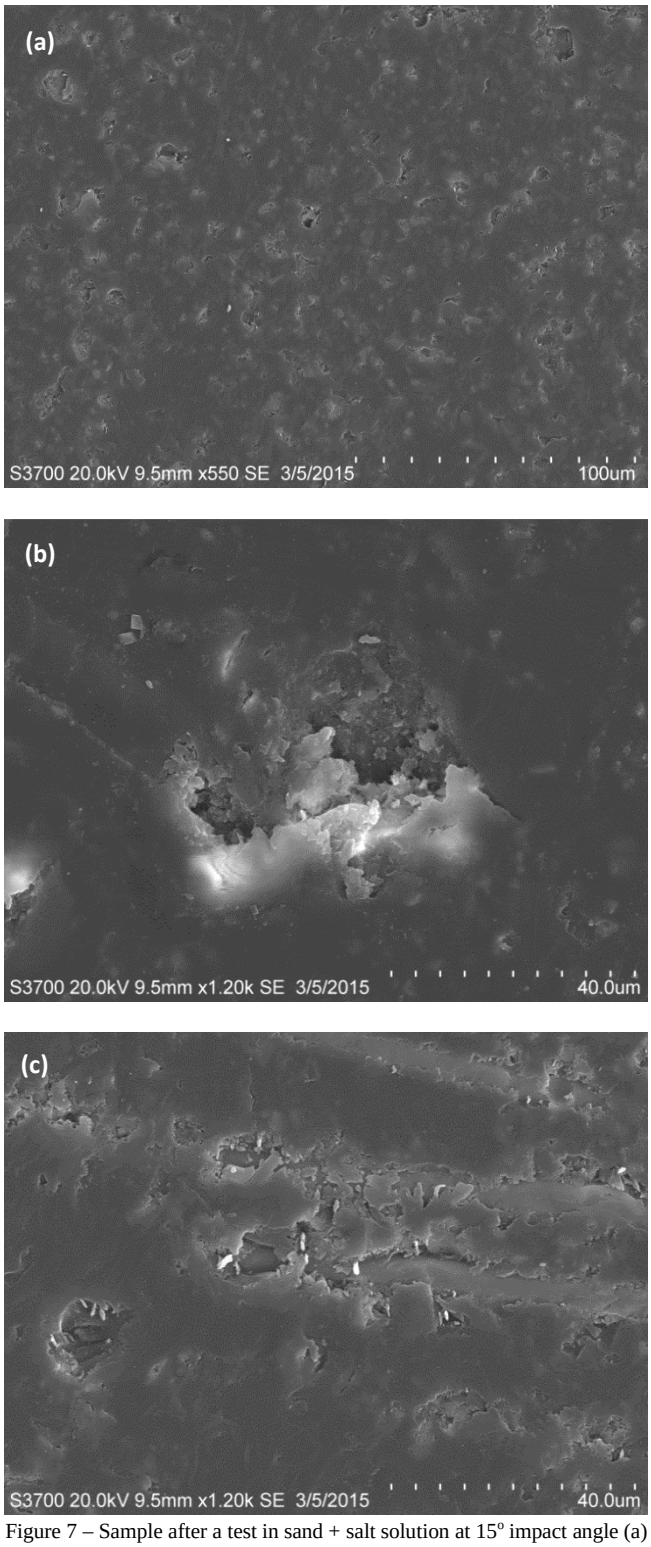

Figure 7 – Sample after a test in sand + salt solution at 15^{o} impact angle (a) site 1, (b) site 2 and (c) site 3

There was not any evidence found indicating the occurrence of erosion under this condition on any of the samples surfaces. However, the evidences of the occurrence of erosion due to the impact of solid particles were clearly observed to different extents on the surfaces of all the samples tested in the solutions contained silica sand particles.

Figure 7 shows three different sites of a sample after a test in sand + salt solution at 15^{o} impact angle. In the wider view (Figure 7(a)), the indentations due to impact of the solid particles can be observed on the specimen surface. In the higher magnification images (Figures 7(b) and 7(c)) the typical effects of erosion on the surface, i.e. platelet formation, can be seen [9]. The platelet formation in the composite materials was observed as flaking due the glossy nature of the surface. It also can be seen that in the areas where the fibres were closer to the surface, the susceptibility to erosion was increased as the fibres are almost exposed. In the real devices, this can be very problematic due to the structural loads on the blades and may result in the breakage of the reinforcement [4].

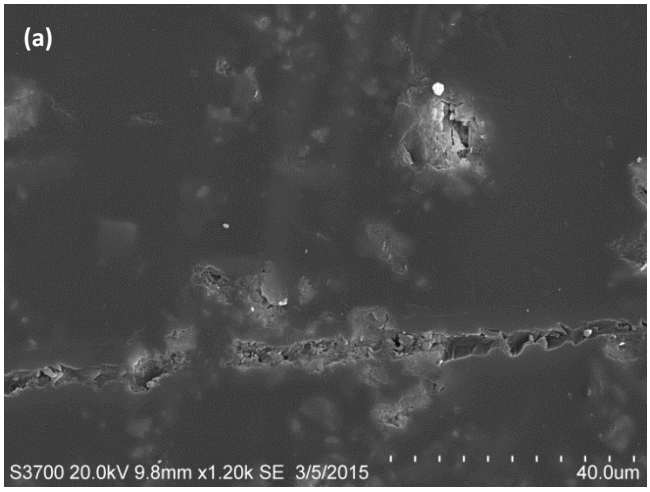

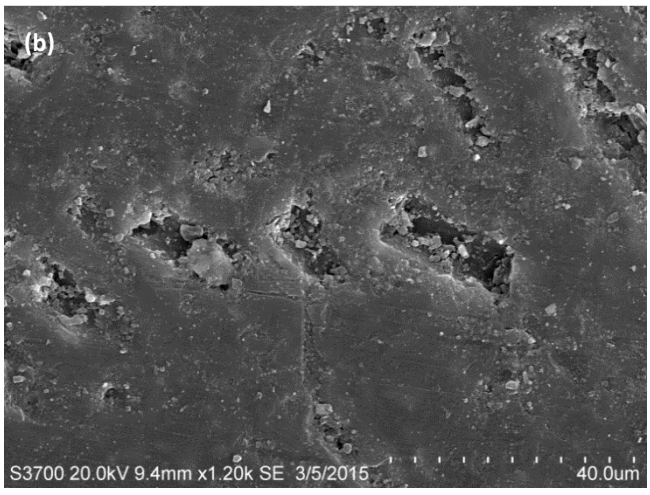

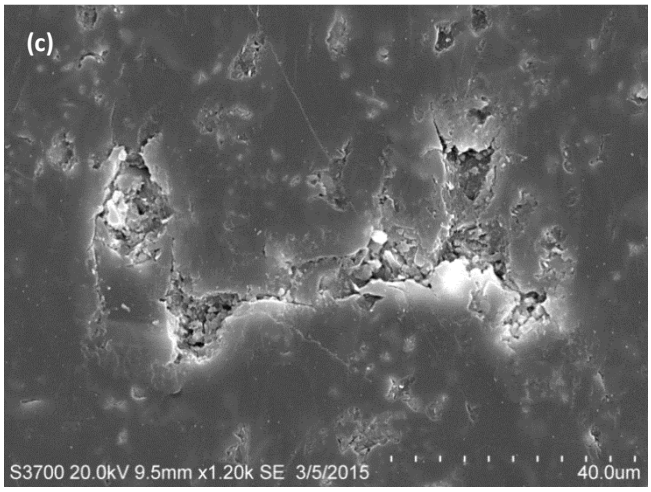

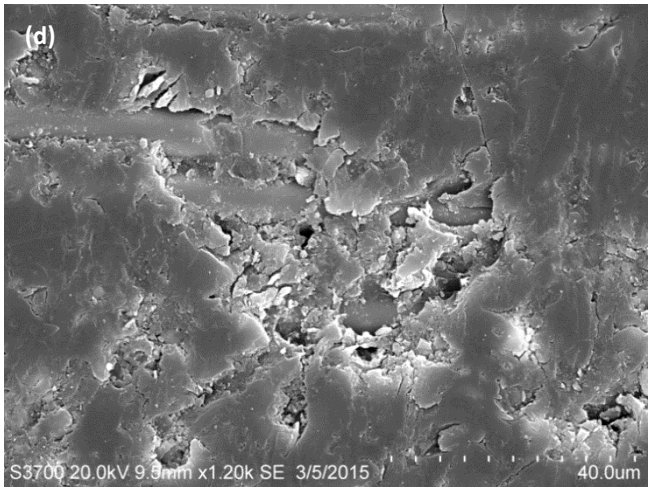

Figure 8 – (a) Different shapes of erosion (b) Sample after a test in sand + salt solution at 15^{o} impact angle (a) site 1, (b) site 2 and (c) site 3

These phenomena were similarly observed on the other samples tested in the presence of the sand particles. Different shapes of erosion were identified on the specimen surfaces. They could be in the shape of indentation marks or scratches as shown in figure 8(a). An interesting observation was the detrimental effects of erosion before and after the crack propagations on the surfaces. There can be a number of indentation sites or pit like structures formed within a close distance due to the impact of particles colliding the surface (Figure 8(b)). These erosion pits became deeper due to the collision of more particles to the dents without causing significant material loss. However, if the pits were in a close distance of each other, once the outer layer of the surface is cracked and the cracks are propagated towards the adjacent dents, the material loss rate accelerated and a significant amount of material will be removed from the surface. This is clearly shown in the images below. Although the images in Figures 8(b), 8(c) and 8(d) are not taken from the same site, this process was repetitively observed on different samples.

IV. DISCUSSION

Solid particle erosion is generally caused by a micro-mechanical/fracture process. On ductile materials it is due to a localised plastic strain which leads to the failure of the deformed material. On brittle materials, the erosion is in a form of cracking and chipping off of the surface in a micro-scale [10]. The erosion damage on the test specimens of this work is due to the erosive action of solid particles suspended in the solution. Although, cavitation can be another cause of erosion, in the current work the blade tip speed and the environment pressure are not suitable for reaching a vapour pressure range and the formation of bubbles, which for the sea water is just above 2 kPa [2], [11]. The flow in the chamber is axial and this is assisted by the four baffle bars that minimised centrifuging of the fluid inside the pot. Also, the concentration of the particles is kept constant for this work. It should be ough thatparticles size, hardness and angularity; however, in higher solid particle concentrations this increase cannot clearly be seen as the kinetic energy of the particles is dissipated partly due to the particle–particle collisions, to the blanketing effect, and to the decrease in particle rotation [8], [12]. As the particles are slowly descending from the top towards the stirring area, it is assumed that the velocity of the particles at time of collision with blade is close to zero and the impact velocity is the velocity of the blade [13]. For the current rig, the velocity differs from the root to the tip of the blades. This is currently under investigation and it is beyond the scope of this paper. The rates of erosion for this work were determined by measuring and averaging the weight loss or gain [8].

The results in Figures 3 and 4 indicate that the erosion rates are higher at the lower impact angles. This is a behaviour that normally observed in ductile materials. According to the literature, the erosion rates of ductile materials typically peaks at a particle impact angle of 30–50 due to occurrence of micro-cutting. The erosion at 90 degrees is caused by deformation wear and Hutchings has suggested that the material loss is observed when a critical fracture strain is reached. It is also stated that the formation and fracture of platelets controls the erosion rate [10], [12]. The peaks of the erosion rate in the current work are observed in the impact angles below 30 degrees which does not completely describe ductile material behaviour (although it should be acknowledged that these impact angles at which the erosion rate peaks can shift depending on the particle characteristics [14]).

According to the literature [9], [15]–[17], composite materials are generally expected to behave as a brittle materials, except for E-glass epoxy composites which perform as a semi-ductile material. This is suggested to be due to better adhesion between the fibres and the matrix and the lower porosity of this type of composites. Zahavi and Schmitt [9] characterised the behaviour of composite materials under solid particle erosion to take place in three stages: (i) local removal of the resin material and exposure of the fibres, (ii) breakage of the fibres and formation of cracks perpendicular to the fibres, and (iii) further damage due to the degradation of the interfaces between the fibres and the resin. The results of the SEM for this work show that these stages are not completely followed for the G10 specimens. As the good adhesion between the components and low porosity of this material are already recognised, only the first stage of this characterisation and to different extents was observed (See Figures 7 and 8). The exposure of the fibres is only observed where they are physically closer to the surface and the resin has protected the fibres and has performed very well as a protectant material.

For metals, the initial erosion rate caused by the first batch of particles is much lower than that of the subsequent batches of erodent. With subsequent increments of impacting particles, the metal loss rate is increased until it reaches steady state conditions where each increment of particles causes the same metal-loss rate to occur. Steady-state conditions occurs after a relatively short exposure period [10].

For the material tested in this work, and as it was mentioned in the previous section, the mechanism of erosion is rather different and a steady state cannot be identified. The impact of the erosive particles causes the formation of platelets and flakes and once the material removal takes place, further impacts result in deepening the erosion pits or micro-cutting. Subsequent impacts in the adjacent surface also take place [18]. This is similar to the behaviour of metals. However, this changes as the resin surfaces is glossy and brittle. The pits within a close distance of each other start to join as the outer layer of the surface begins to crack and propagate. The connections formed between the dents through the cracks accelerate the material removal and the mass loss becomes significant.

Another factor which is observed from the results is the effects of the dissolved salt in the water on the wear performance of the G10 composite. Referring to Figure 4, the amplitude of the deviations of the weight gain due to the presence of salt in the water in the salt only tests is rather small comparing to the other tests. On average, each sample has gained 0.011% of its initial weight after the tests. By deducting this value from the final weight of the tests with salt + sand, pure erosion can be calculated. Pure erosion in such

conditions has been plotted in the Figure 9. The curve in Figure above follows the same trend as the pure erosion results with higher mass loss in smaller blade angles.

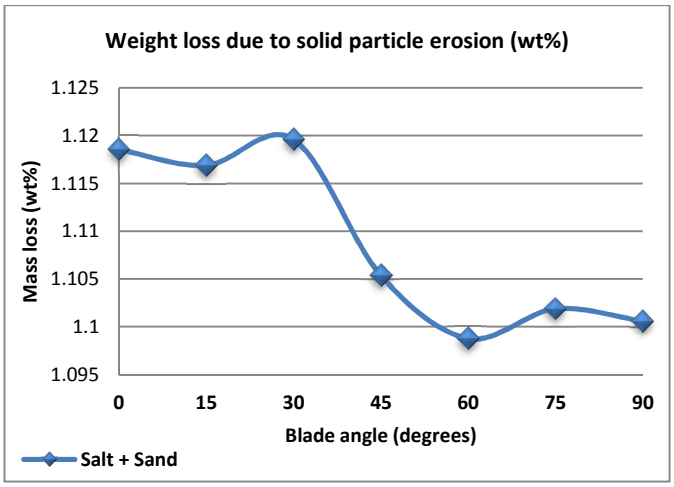

Figure 9 - Weight loss due to solid particle erosion in the Sand + salt solution (wt%)

If the results for the pure erosion in the sand only solution and the pure erosion from the sand + salt are plotted in a same graph, it indicates that the presence of salt has significantly increased the amount of erosion (See Figure 10). The curve plotting the erosion in the sand + salt solution has clearly shifted upwards. This emphasises the deteriorating effects of salt on tribological performance of materials and the importance of synergistic effects of salt and sand. Hence, using methods to avoid the absorption of salt seems to be necessary in order to optimize material performance.

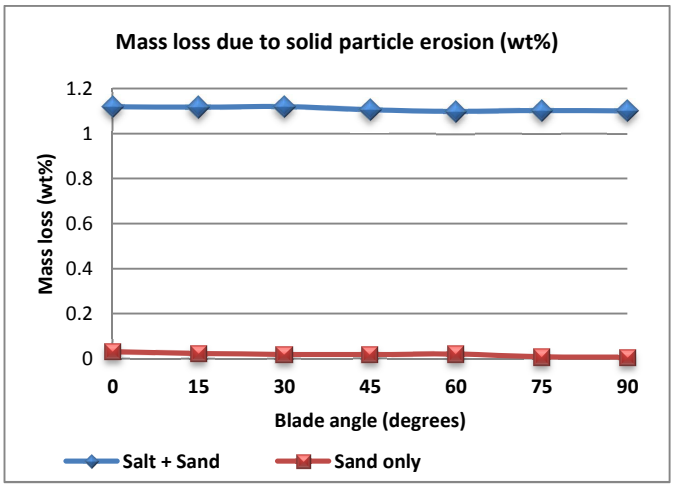

Figure 10 – Weight loss comparison due to erosion in Sand only and Sand + Salt solutions

It is observed in the SEM that the salt crystals are mainly absorbed and accumulated where the fibres are closer to the surface. Also, as it is demonstrated in the work and is documented in the literature, the exposure of fibres can be very problematic and increases the susceptibility of the material to be eroded or result in failure due to the lack support from the protectant material. Therefore, using surface coating or gel coats for such materials can enhance the quality of performance and the life span of such materials. Further work will involve assessing the performance of different gel coats, reinforcements lay-outs and reinforcements volume fractions in order to optimize the composite for exposure to the operating environment.

V. CONCLUSIONS

An investigation of the solid particle erosion behaviour of G10 epoxy E-glass laminate as a potential candidate material for turbine blades resulted in the following conclusions:

(i) The erosion wear performance of GFRP materials is similar to a semi-ductile material in the conditions tested.

(ii) The presence of salt while the material is being eroded exacerbates the erosion rate

(iii) The higher erosion rates for G10 epoxy E-glass laminate were observed in the impact angles between 0-30 degrees.

(iv) A good surface finish is crucial for a material to perform well under erosion

(v) Composite materials subjected to erosion should be coated in order to avoid/delay the hazardous exposure of the reinforcing fibres

ACKNOWLEDGEMENTS

The authors would like to acknowledge the support of the EPSRC Supergen Grand Challenges Grant No EP/K013319/1, “Reducing the Costs of Marine Renewables via Advanced Structural Materials (ReC-ASM)” and thank The Advanced Materials Group in Newcastle University for providing the test samples.

REFERENCES

[1] I. E. A. R. E. T. D. (IEA-RETD), *Offshore Renewable Energy: Accelerating the Deployment of Offshore Wind, Tidal, and Wave Technologies*. Routledge, 2011, p. 328.

[2] D. M. Grogan, S. B. Leen, C. R. Kennedy, and C. M. Ó Brádaigh, “Design of composite tidal turbine blades,” *Renew. Energy*, vol. 57, pp. 151–162, 2013.

[3] J. N. Goundar and M. R. Ahmed, “Design of a horizontal axis tidal current turbine,” *Appl. Energy*, vol. 111, pp. 161–174, Nov. 2013.

[4] P. Blau and R. Divakar, *Wear testing of advanced materials*. Philadelphia Pa.: American society for testing and materials, 1992, p. 170.

[5] A. A. Gadhikar, A. Sharma, D. B. Goel, and C. P. Sharma, “Fabrication and Testing of Slurry Pot Erosion Tester,” *Trans. Indian Inst. Met.*, vol. 64, no. 4–5, pp. 493–500, Dec. 2011.

[6] A. Abouel-Kasem, Y. M. Abd-elrhman, K. M. Emara, and S. M. Ahmed, “Design and Performance of Slurry Erosion Tester,” *J. Tribol.*, vol. 132, no. 2, p. 021601, Apr. 2010.

[7] G. R. Desale, B. K. Gandhi, and S. C. Jain, “Improvement in the design of a pot tester to simulate erosion wear due to solid–liquid mixture,” *Wear*, vol. 259, no. 1–6, pp. 196–202, Jul. 2005.

[8] W. Tsai, J. A. C. Humphrey, I. Cornet, and A. V. Levy, “Experimental measurement of accelerated erosion in a slurry pot tester,” *Wear*, vol. 68, no. 3, pp. 289–303, May 1981.

[9] J. Zahavi and G. F. Schmitt, “Solid particle erosion of reinforced composite materials,” *Wear*, vol. 71, no. 2, pp. 179–190, Sep. 1981.

[10] A. V. Levy, *Solid Particle Erosion and Erosion-corrosion of Materials*. ASM International, 1995, p. 220.

[11] H. J. Amarendra, G. P. Chaudhari, and S. K. Nath, “Synergy of cavitation and slurry erosion in the slurry pot tester,” *Wear*, vol. 290–291, pp. 25–31, Jun. 2012.

[12] M. Lindgren and J. Perolainen, “Slurry pot investigation of the influence of erodent characteristics on the erosion resistance of austenitic and duplex stainless steel grades,” *Wear*, vol. 319, no. 1–2, pp. 38–48, Nov. 2014.

[13] K. K. Wong and H. M. Clark, “A model of particle velocities and trajectories in a slurry pot erosion tester,” *Wear*, vol. 160, no. 1, pp. 95–104, Jan. 1993.

[14] B. D. Jana and M. M. Stack, “A note on threshold velocity criteria for modelling the solid particle erosion of WC/Co MMCs,” *Wear*, vol. 270, no. 7–8, pp. 439–445, Mar. 2011.

[15] K. V. Pool, C. K. H. Dharan, and I. Finnie, “Erosive wear of composite materials,” *Wear*, vol. 107, no. 1, pp. 1–12, Jan. 1986.

[16] G. P. Tilly and W. Sage, “The interaction of particle and material behaviour in erosion processes,” *Wear*, vol. 16, no. 6, pp. 447–465, Dec. 1970.

[17] M. Roy, B. Vishwanathan, and G. Sundararajan, “The solid particle erosion of polymer matrix composites,” *Wear*, vol. 171, no. 1–2, pp. 149–161, Jan. 1994.

[18] S. S. Rajahram, T. J. Harvey, and R. J. K. Wood, “Electrochemical investigation of erosion–corrosion using a slurry pot erosion tester,” *Tribol. Int.*, vol. 44, no. 3, pp. 232–240, Mar. 2011.